Optics and Lasers in Engineering 161 (2023) 107393

Contents lists available at ScienceDirect

Optics and Lasers in Engineering

journal homepage: www.elsevier.com/locate/optlaseng

Spectra-separated depth-of-field extended fluorescence imaging through scattering media using speckle deconvolution

Xiaodong Wang [a], Dayan Li [a,*], Zhihe Liu [a], Xiaofeng Fang [a], Jiani Li [a], Tianyue Shi [a], Changfeng Wu [a,b]

[a] Department of Biomedical Engineering, Southern University of Science and Technology, Shenzhen, Guangdong 518055, China
[b] Shenzhen Bay Laboratory, Shenzhen, 518132, China

ARTICLE INFO

Keywords:
Fluorescence imaging
Scattering media
Deconvolution imaging
Speckle pattern

ABSTRACT

Over the last decade, many methods have been proposed to achieve optical imaging through scattering media. Among them, speckle deconvolution utilizing the optical memory effect of the medium is widely employed due to its advantages in imaging speed and relatively simpler setup. However, practical applications of speckle deconvolution method are rarely demonstrated as most of the existing systems are based on transmission geometry to ensure direct incoherent illumination and easy detection. Here we propose an imaging system in reflection configuration that is able to retrieve the hidden fluorescent object behind a thin scattering media by speckle deconvolution. The object speckle pattern and speckle pattern from a point source (point spread function of the system, PSF) are spectrally separated to facilitate non-invasive image acquisitions. It is shown that, to reconstruct object faithfully, spectral de-correlation and chromatic aberration induced depth de-correlation between the object speckle pattern and the PSF have to be compensated. Speckle correlation is employed to characterize the depth-of-field (DOF) range in this reflection imaging system. Within the DOF, focus and defocus effects in the reconstructed objects are observed when rescaling the PSF onto different axial planes. Beyond the DOF, hidden objects that originally fail in reconstruction can be retrieved by PSF stacking and PSF rescaling. The proposed approach is potentially to find wide applications in biomedical imaging, ranging from deep tissue fluorescence microscopy to small animal imaging.

1. Introduction

Light scattering in heterogeneous media scrambles the incident and outgoing wave-front, producing a noise-like speckle pattern that buries object image. This is particularly problematic for biological applications, such as fluorescence imaging in deep tissues. To address this problem, several techniques have been proposed in order to compensate the scattering effect and retrieve clear images. For example, one can utilize wave-front shaping [1] or optical phase conjugation [2] to find the optimized wave-front that corrects the wave distortions. Another powerful approach is transmission matrix [3]. Transmission matrix models the wave propagation (including light scattering effect) as a linear matrix where the relationships between the input and output modes are established. While the techniques mentioned above are very promising in compensating the scattering effect, they usually require either long measurement time (need a series of measurements to characterize the media) or complicated setup (e.g. interferometry to measure the optical fields).

In order to realize instant imaging through scattering media with relatively simple optical system and a few prior characterizations of the scattering medium, optical memory effect (OME) based phase retrieval method [4,5] and speckle deconvolution [6] were developed. Optical memory effect [7] states that a seemingly random speckle pattern after scattering media is highly correlated with the one generated when incident light is tilted a small angular angle. Due to this shift-invariant property, within the OME range speckle pattern for an object can be mathematically modeled as the convolution between the object and system PSF. Phase retrieval from speckle autocorrelation appeals to be a promising approach for single shot and non-invasive imaging since it requires neither complicated optics nor prior information. However, it is more vulnerable to low 'signal to noise ratio' (SNR) compared to the speckle deconvolution approach. Deconvolution imaging through scattering media has been demonstrated with high-resolution [6], fast imaging [8] and spectral discrimination ability [9,10]. Many works are devoted to extend the system's field-of-view [11–16] and depth-of-field [17,18]. Nevertheless, most of the proposed deconvolution based optical

* Corresponding author.
E-mail address: lidy7@mail.sustech.edu.cn (D. Li).

https://doi.org/10.1016/j.optlaseng.2022.107393
Received 30 August 2022; Received in revised form 23 October 2022; Accepted 14 November 2022

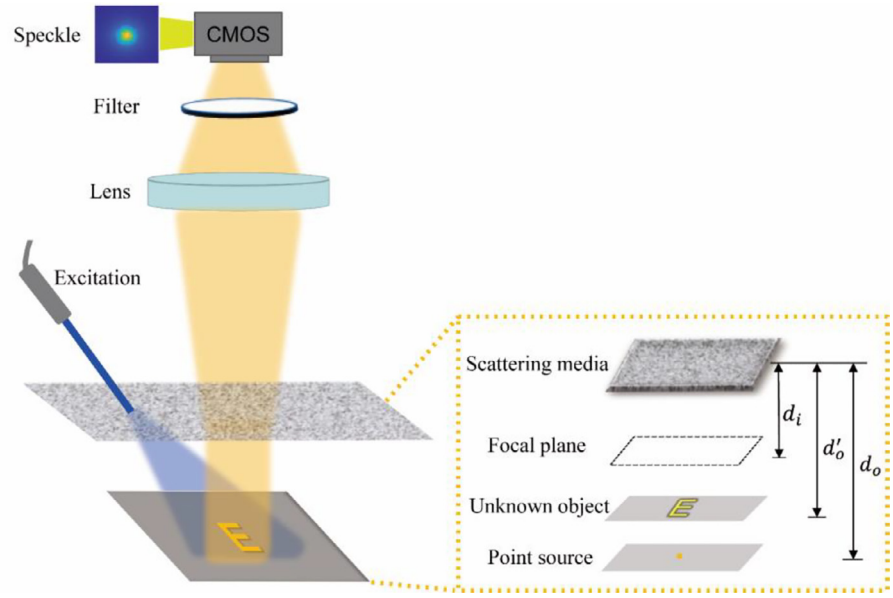

Fig. 1. Schematic diagram of the optical system employed for imaging through scattering media.

systems are employing transmission geometry to facilitate illumination and detection, which is not compatible with fluorescence imaging [6-15,17,18]. To the best of our knowledge, fluorescence imaging behind a scattering media in reflection configuration enabled by deconvolution has not been reported yet [19–22].

In this work, we propose a reflective imaging system that can retrieve the hidden fluorescent object behind a thin scattering media by speckle deconvolution. In order to facilitate the non-invasive acquisitions of object speckle and the PSF of system, a home-designed wheel for optical filtering is incorporated. Dual-color fluorescence is used, as a result, object speckle and the system PSF can be separated spectrally. We characterize the depth-of-field (DOF) range of the system using speckle correlation. Within the DOF, focus and defocus effects in the reconstructed objects are observed by simply rescaling the PSF onto different axial planes. Finally, using PSF stacking and PSF scaling, we show that fluorescence imaging beyond the DOF range can be realized.

2. Principles

The scheme of imaging through a thin scattering layer in a reflection configuration is illustrated in Fig. 1. A fluorescence object located behind a scattering layer is excited by a laser beam, which is placed at the same side as the camera. An imaging optic composed of a single lens and filters are introduced to capture the fluorescence signal through the scattering media. The distance between object (or point source) and scattering media is denoted by d_o (or d'_o) while the distance between focal plane and scattering media is denoted by d_i. Now, suppose that a point source at the object plane generates a speckle-like pattern representing the PSF of this imaging system. This PSF exhibits a linear shift-invariant property within the OME range. In this way, the speckle pattern originating from an object will be the incoherent superimposition of the PSF weighted by the object. Thus, the object speckle pattern I captured in the camera plane is mathematically represented by,

$$I(x_i, y_i) = O(x_o, y_o) * PSF(x_i, y_i; x_o, y_o) \tag{1}$$

where the subscript i and o denote the object plane and image plane, respectively, and $*$ represents the convolution operator. Therefore, once we obtain the PSF and object speckle I, the hidden object behind the scattering media can be reconstructed by deconvolution algorithm, $O = deconv(I,\ PSF)$. Wiener deconvolution is used in this paper for image reconstruction.

As reported in literature [10], PSFs from various axial planes and wavelengths share the same function except the scaling in transform variable, which yields PSF_u at specific depth or wavelength,

$$PSF_u(x, y) \approx m^2 PSF(mx, my) \tag{2}$$

where m represents the scaling factor at specific depth and wavelength. For depth scaling factor [17],

$$m_d = (di/do + 1)/\left(di/d'_o + 1\right). \tag{3}$$

As a result, if the unknown object and point source are located at different axial planes, depth scaling factor m_d could be used to rescale the PSF onto the object plane.

Similarly, spectral scaling factor could be defined as,

$$m_\lambda = \frac{\lambda_{object}}{\lambda_{psf}} \tag{4}$$

where λ_{object} and λ_{psf} are the wavelengths of object fluorescence and point source fluorescence, respectively. When both depth difference and spectral difference exist, the total scaling factor would be $m = m_d \times m_\lambda$.

3. Results

3.1. Fluorescence imaging through scattering media via spectra and depth compensation

We home-built an inverted fluorescence imaging system, see Supplement 1 for detailed descriptions. Two optical filters (BP540nm and BP650nm) are installed in the filter wheel . The bandwidths of the two filters are both 45 nm, as shown in Fig. 2(a). In this experiment, DTE-PFDTBT and PFBT polymer dots are selected to respectively make red point source and yellow object. Both fluorescent materials are placed at the same depth and excited by a 488 nm laser simultaneously. We sequentially record the object speckle pattern under BP540nm filter (Fig. 2c) and the PSF under BP650nm (Fig. 2d), by only rotating the home-designed filter wheel. Our system has the advantage that the point source and object can be simultaneously illuminated, and they are discriminated simply by filters. Therefore, the standard characterization procedure (measuring PSF in advance) in speckle deconvolution is eliminated.

The spectral scaling factor is around 1.20 (m_λ=650/540=1.20). In addition, in the lens-based imaging system, chromatic aberration

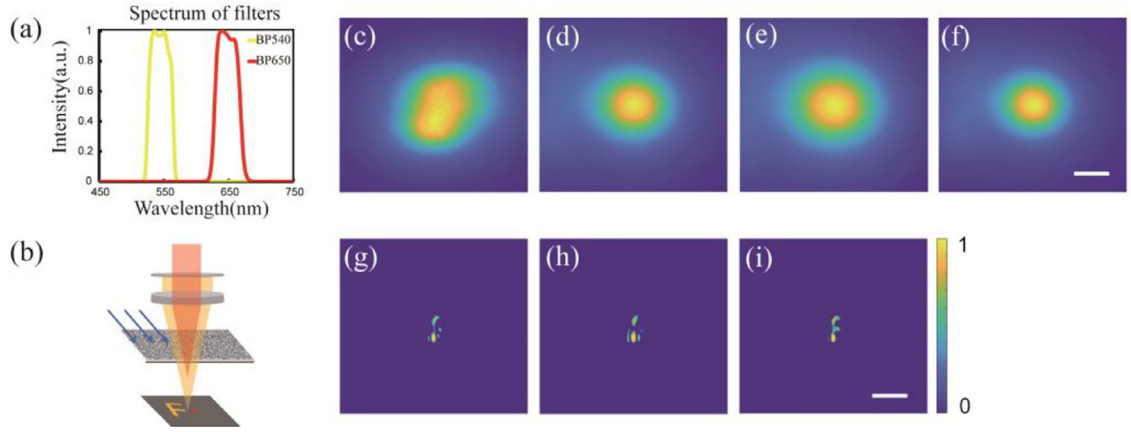

Fig. 2. Fluorescence imaging through a thin scattering medium via spectra and depth compensation. (a) Spectrum of BP540 and BP650. (b) Schematic of dual-color imaging at the same depth. (c) Object speckle under BP540. (d) PSF under BP650. (e) Rescaled PSF with spectral scaling factor m_λ = 1.20. (f) Rescaled PSF with both spectral scaling and depth scaling are considered, m = $m_d \times m_\lambda$ =0.86. (g) Deconvolution between (c) and (d). (h) Deconvolution between (c) and (e). (i) Deconvolution between (c) and (f). Scale bars in (c-f) are 250 μm. Scale bars in (g-i) are 1.422 mm.

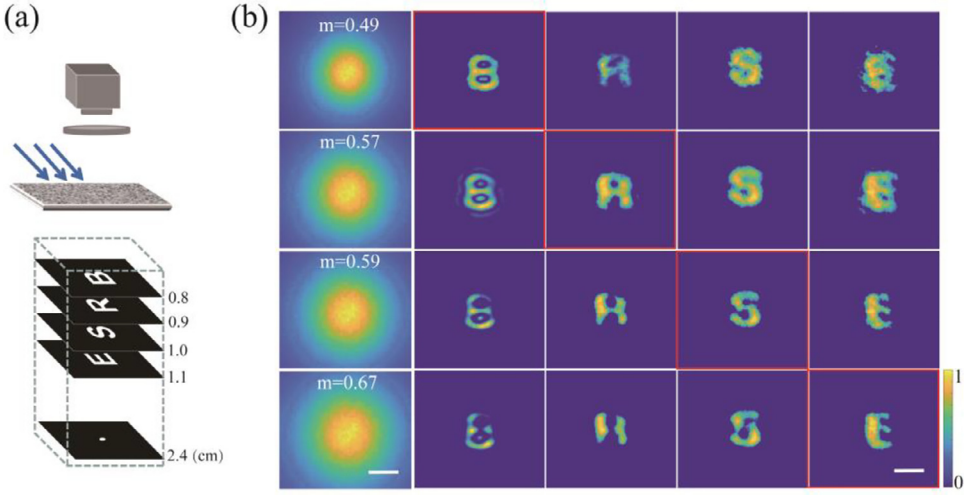

Fig. 3. Focus and defocus effects via PSF scaling. (a) Schematic illustration. (b) The first column is the rescaled PSFs by scaling the reference PSF (d_o=2.4 cm) to different axial planes. The second to fifth column show the retrieved images corresponding to different axial planes by speckle deconvolution. The scale bars in (b) are 200 μm, 500 μm, respectively.

[22] will be presented and light from different wavelengths has different focal planes, as illustrated in Fig. 2(b). The chromatic aberration induced depth difference must be compensated as well. Mathematically, by monitoring the quality of reconstructed image as a function of total scaling factor, we could find the optimized m for our system. Nevertheless, we conducted thorough measurements to verify the compensation theory outlined above.

The focal planes for the two wavelengths are measured in advance to be d_r=0.65 cm and d_y=1.15 cm, respectively. This is achieved by moving the multi-axis translation stage along the depth direction, and searching for the best focal planes using corresponding fluorescent objects. After measuring the chromatic aberration induced defocus, both red point source and unknown yellow object are placed at a depth (d_y=1.15 cm). The defocus effect caused by the chromatic aberration can be considered as a new form of depth difference, where d_o'=d_r=0.65 cm, d_o=d_i=d_y=1.15 cm, thus giving m_d=0.72. Therefore, the total scaling factor is given m=$m_d \times m_\lambda$=0.86.

The PSFs in Fig. 2(d-f) represent the rescaled PSFs with scaling factors of 1.00, 1.20, and 0.86, respectively. Obviously when compensating only the spectral de-correlation, the reconstruction (Fig. 2h) fails to restore the hidden object. However, when taking both the spectral and depth de-correlation into account, speckle deconvolution leads to a well-reconstructed image (Fig. 2i). The restored image has a significant improvement compared to the reconstruction without PSF scaling (Fig. 2g). These results demonstrate the necessity in compensating both the spectral and depth de-correlation in speckle deconvolution.

3.2. PSF rescaling enabled focus and defocus effects

The fluorescence imaging system is further investigated for three-dimensional (3D) reconstruction, as is presented in Fig. 3. Here we set the focal plane and plane of PSF at the same depth, d_o=d_i=2.4 cm. By recording only one reference PSF and rescaling this PSF onto different axial planes, a series of virtual PSFs are generated. Object speckle patterns are captured various axial planes, with object-diffuser distance d_o' = 0.8 cm, 0.9 cm, 1.0 cm, 1.1 cm. As the object reconstruction results are shown in Fig. 3(b). Each rescaled PSF (scaling factor m = 0.49, 0.57 0.59, 0.67) deconvolving with object speckle patterns at different planes leads to one row in Fig. 3(b). The red box highlights the corresponding targeted depth for each rescaled PSF. The results demonstrate that refocused imaging through the scattering media was enabled by PSF scaling, which facilitates the reconstruction of 3D object. However, due to the large depth-of-field (DOF) of the system, a 3D object within the DOF cannot be totally depth resolved. We will investigate the system's DOF in next section.

3.3. Characterizing the system's depth-of-field (DOF)

To measure the system's DOF, a series of PSFs in different axial planes are recorded, by translating a point source along the optical axis at a step size 0.025 cm. We cross-correlate the PSFs and fit the correlation values using on-axis correlation function of speckle patterns. For speckles generated with Gaussian pupil function, the on-axis correlation function is

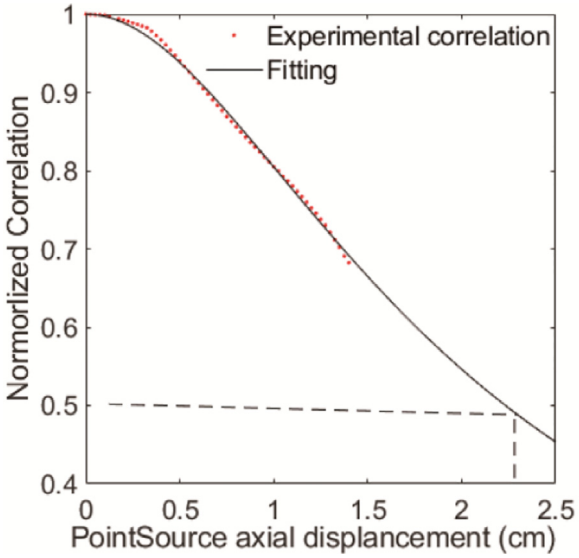

Fig. 4. Normalized correlation between PSFs recorded at different axial planes. Red points: experimental correlation values; Black curve: fitting by using Eq. (5).

given by [23]

$$\mu_{12} = \frac{1}{1 + \left(d_z / l_z\right)^2} \tag{5}$$

where μ_{12} is the on-axis correlation value between axial plane 1 and plane 2, d_z is the distance between the two planes, and $l_z = 4d_0(d_o+d_z)/(w^2k)$, with w and k are the illumination beam size and wavenumber, respectively. In this experiment, the point source plane is set at a depth of d_o =1.15 cm. The fitting of Eq. (5) to the experimental data is shown by black curve in Fig. 4. DOF is commonly characterized by its full width at half the maximum (FWHM) value [24], which is 2.3 cm in our case. As a result, the objects studied in Fig. 3 are all laying within the DOF of the system, which makes them difficult to be fully discriminated in depth. Nevertheless, PSF scaling will find the depth at which the object is in focus.

The fitted curve in Fig. 4 gives us the nominal DOF of the system, which is 2.3 cm. In practice, higher axial correlation is required to guarantee a faithful object reconstruction. In order to determine the DOF value in practice, further characterization of DOF is performed using deconvolution. We measured a series of PSF and speckle patterns at different axial planes, starting from a depth $d_o = d'_o = 0.8$ cm, with a step size of 0.1 cm. The reconstructions are thereafter obtained by deconvolution, as shown in Fig. 5(a-f). We see that the reconstructed image deteriorates as object-diffuser distance d'_o increases. More importantly, when the object is placed at a distance larger than 1.2 cm, we observe obvious deteriorating parts of letter 'E'. This indicates that the object is located beyond the DOF range. Object-diffuser distance d'_o also affects the magnification of the imaging systems. We see that, as object-diffuser distance increases, reconstructed objects are magnified and defocused. From these reconstruction results, we could infer that the system's DOF is about $d_z = 0.5$ cm. 0.5 cm is a value much less than the nominal DOF.

3.4. *Fluorescence imaging through scattering media beyond DOF of the system*

In order to address the limited depth-of-field (DOF) problem, PSF manipulation based on stacking and scaling are exploited, respectively. In the first experiment, as shown in Fig. 6(a), by recording and averaging a series of nearby PSFs, a stacked PSF is produced to replace the original PSF. We capture the PSF (Fig. 6b) and object speckle at the same depth (d_o=d'_o=1.35 cm) that is beyond the system's DOF. The reconstruction by speckle deconvolution is shown in Fig. 6(d). By collecting PSFs from d_o=0.8 cm to d_o=1.35 cm with a step size of 0.05 cm, a stacked PSF is generated (Fig. 6c). The reconstruction with this stacked PSF is shown in Fig. 6(e), where the missing parts of letter 'E' are restored to some extent. It indicates that with PSF stacking the limited DOF can be counteracted and therefore enabling extended DOF imaging.

PSF stacking can extend the DOF of the optical system, however, this process requires multiple PSF acquisitions. To simplify this process, the second experiment explores the inherent depth correlation of PSFs by PSF scaling. The virtual PSF after scaling is used to substitute the original PSF for deconvolution imaging. Fig. 7(a) shows a schematic diagram of the PSF scaling operation. In our setup the image plane is set at a depth of $d_i = 1.15$ cm, and the object-diffuser distance is $d'_o = 1.35$ cm.

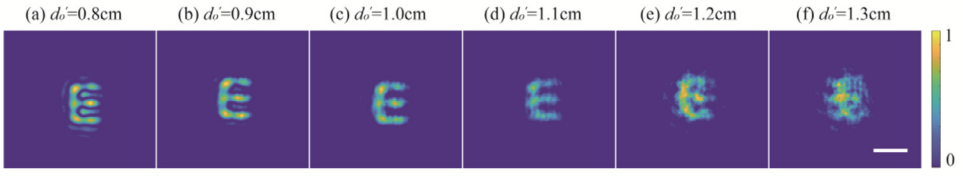

Fig. 5. Effect of the object-diffuser distance on deconvolution reconstruction. (a)-(f): Deconvolution reconstruction with different object-diffuser distances from 0.8 cm to 1.3 cm with a step size of 0.1 cm. The scale bars in (a-f) are 500 μm.

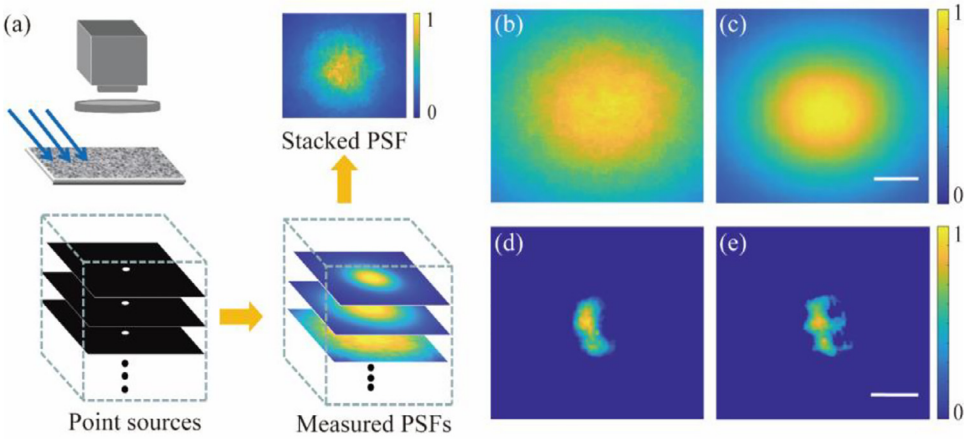

Fig. 6. Imaging beyond DOF via PSF stacking. (a) Schematic of PSF stacking. (b) PSF captured at d_o=1.35 cm. (c) Stacked PSF generated from d_o=0.8 cm to d_o=1.35 cm with a step size of 0.05 cm. (d) Deconvolution of object speckle (d'_o=1.35 cm) and PSF (d_o=1.35 cm). (e) Deconvolution of object speckle (d'_o=1.35 cm) and stacked PSF (d_o=0.8~1.35 cm). The scale bar in (c) and (b) is 100 μm. The scale bar in (d) and (e) is 500 μm.

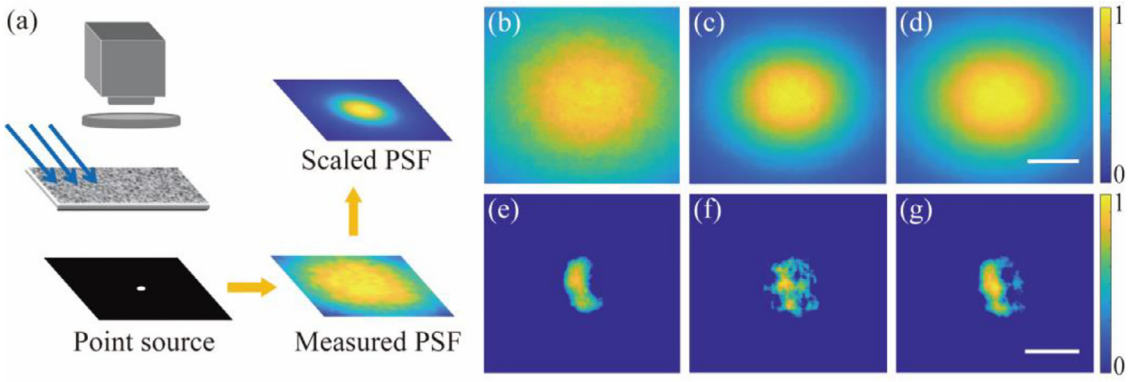

Fig. 7. Imaging beyond DOF via PSF scaling. (a) Schematic of PSF scaling. (b) PSF captured at d_o=1.35 cm. (c) PSF captured at d_o=0.8 cm. (d) Scaled version of PSF at d_o=0.8 cm (m = 1.3). (e-f) Deconvolution of object speckle with corresponding PSFs in (b-d). The scale bar in (d) is 100 μm and also applies to (b) and (c). The scale bar in (g) is 500 μm and also applies to (e) and (f).

PSF is captured at a depth of d_o = 0.8 cm, leading to m = 1.32. Fig. 7(b) and Fig. 7(c) are, respectively the PSFs captured at d_o = 1.35 cm and d_o = 0.8 cm, and Fig. 7(d) is the scaled version of PSF at d_o=0.8 cm. Speckle deconvolution by the above three PSFs is performed sequentially with the same object speckle at d_o'=1.35 cm. As shown in Fig. 7(g), we manage to reconstruct the hidden 'E' letter, whereas the original reconstruction that beyond the DOF fails.

4. Conclusion and discussions

In conclusion, we have constructed a reflective imaging system and demonstrated fluorescence imaging through a thin scattering medium via speckle deconvolution. To facilitate non-invasive acquisitions of both the object speckle pattern and the PSF, we developed and utilized fluorescence in separated wavelength channel. Due to chromatic aberration, in this case it requires both depth and wavelength de-correlation compensation to maintain maximum reconstruction performance. By the virtue of depth correlation of PSFs in different axial planes, focus and defocus effects in object reconstruction were demonstrated. More interestingly, it is found that the DOF in our imaging system can be extended by either PSF stacking or PSF scaling. We validated this point by reconstructing the objects hidden behind a thin scattering medium that was originally located outside the DOF of the imaging system.

We provided additional experiment that is relevant to biomedical imaging in the supplementary document. We must admit that so far real data on biomedical imaging is not provided yet. This is mainly due to the difficulty in creating single point source inside animal body. Our future work will focus on the practical applications and limitations of the system on biomedical imaging. Noticed that many other schemes are proposed recently to achieve non-invasive imaging through scattering media, including speckle correlation [25], single-pixel imaging [26,27] and deep learning [28]. They are all with the goal to purse real applications in biomedical field in the end. We expect our work will convey contributions to this ultimate goal.

Author Statement

Xiaodong Wang: Experiments, Sample preparation, Data curation, Writing–original draft. **Dayan Li:** Conceptualization, Supervision, Writing – review & editing. **Zhihe Liu:** Optical setup. **Xiaofeng Fang:** Sample preparation. **Jiani Li & Tianyue shi:** Validation. **Changfeng Wu:** Instruction and supervision.

Declaration of Competing Interest

The authors declare that they have no known competing financial interests or personal relationships that could have appeared to influence the work reported in this paper.

Data Availability

Data will be made available on request.

Funding

This work was supported by National Key R&D Program of China (2020YFA0909000); Shenzhen Science and Technology Innovation Commission (KQTD20170810111314625 & JCYJ20210324115807021); National Natural Science Foundation of China (81771930); Open Fund of the State Key Laboratory of Integrated Optoelectronics (IOSKL2020KF13) and Shenzhen Bay Laboratory (SZBL2021080601002).

Supplementary materials

Supplementary material associated with this article can be found, in the online version, at doi:10.1016/j.optlaseng.2022.107393.

References

[1] Vellekoop IM, Mosk AP. Focusing coherent light through opaque strongly scattering media. Opt Lett 2007;32(16):2309–11.
[2] Yaqoob Z, Psaltis D, Feld MS, Yang C. Optical phase conjugation for turbidity suppression in biological samples. Nat Photonics 2008;2(2):110–15.
[3] Popoff SM, Lerosey G, Carminati R, Fink M, Boccara AC, Gigan S. Measuring the transmission matrix in optics: an approach to the study and control of light propagation in disordered media. Phys Rev Lett 2010;104(10):100601.
[4] Bertolotti J, van Putten EG, Blum C, Lagendijk A, Vos WL, Mosk AP. Non-invasive imaging through opaque scattering layers. Nature 2012;491(7423):232–4.
[5] Katz O, Heidmann P, Fink M, Gigan S. Non-invasive single-shot imaging through scattering layers and around corners via speckle correlations. Nat Photonics 2014;8(10):784–90.
[6] Edrei E, Scarcelli G. Memory-effect based deconvolution microscopy for super-resolution imaging through scattering media. Sci Rep 2016;6(1):33558.
[7] Freund I, Rosenbluh M, Feng S. Memory effects in propagation of optical waves through disordered media. Phys Rev Lett 1988;61(20):2328–31.
[8] Zhuang H, He H, Xie X, Zhou J. High speed color imaging through scattering media with a large field of view. Sci Rep 2016;6(1):32696.
[9] Sahoo SK, Tang D, Dang C. Single-shot multispectral imaging with a monochromatic camera. Optica 2017;4(10):1209–13.
[10] Xu X, Xie X, Thendiyammal A, Zhuang H, Xie J, Liu Y, et al. Imaging of objects through a thin scattering layer using a spectrally and spatially separated reference. Opt Express 2018;26(12):15073–83.
[11] Tang D, Sahoo SK, Tran V, Dang C. Single-shot large field of view imaging with scattering media by spatial demultiplexing. Appl Opt 2018;57(26):7533–8.
[12] Zhu X, Kumar Sahoo S, Wang D, Quoc Lam H, Anthony Surman P, Li D, et al. Single-shot multi-view imaging enabled by scattering lens. Opt Express 2019;27(26):37164–71.
[13] Wang X, Jin X, Li J, Lian X, Ji Xi, Dai Q. Prior-information-free single-shot scattering imaging beyond the memory effect. Opt Lett 2019;44(6):1423–6.
[14] Li W, Liu J, He S, Liu L, Shao X. Multitarget imaging through scattering media beyond the 3D optical memory effect. Opt Lett 2020;45(10):2692–5.
[15] He W, Wei Y, Lu D, Li X, Liao M, Peng X. Noninvasive imaging of two isolated objects through a thin scattering medium beyond the 3D optical memory effect by speckle-based difference strategy. Opt Lett 2021;46(23):5954–7.

[16] Zhu L, Soldevila F, Moretti C, d'Arco A, Boniface A, Shao X, et al. Large field-of-view non-invasive imaging through scattering layer using fluctuating random illumination. Nat Commun 2022;13:1447.
[17] Xie X, Zhuang H, He H, Xu X, Liang H, Liu Y, Zhou J. Extended depth-resolved imaging through a thin scattering medium with PSF manipulation. Sci Rep 2018:4585.
[18] Liao M, Lu D, Pedrini G, Osten W, Situ G, He W, et al. Extending the depth-of-field of imaging systems with a scattering diffuser. Sci Rep 2019;9(1):7165.
[19] Chang J, Wetzstein G. Single-shot speckle correlation fluorescence microscopy in thick scattering tissue with image reconstruction priors. J Biophotonics 2018;11(3):e201700224.
[20] Hofer M, Soeller C, Brasselet S, Bertolotti J. Wide field fluorescence epi-microscopy behind a scattering medium enabled by speckle correlations. Opt Express 2018;26(8):9866–81.
[21] Yoon S, Kim M, Jang M, Choi Y, Choi W, Kang S, et al. Deep optical imaging within complex scattering media. Nat Rev Phys 2020;2(3):141–58.
[22] Zhao F, Du S, Liang D, Liu J. Simultaneously improving multiple imaging parameters with scattering media. Appl Opt 2021;60(21):6091–6.
[23] Li D, Kelly DP, Sheridan JT. Three-dimensional static speckle fields. Part I. Theory and numerical investigation. J Opt Soc Am 2011;28(9):1896–903.
[24] Goodman JW. Speckle phenomena in optics: theory and applications. Englewood, Colorado: Roberts & Company; 2007. p. pp84.
[25] kamoto Y, Horisaki R, Tanida J. Noninvasive three-dimensional imaging through scattering media by three-dimensional speckle correlation. Opt Lett 2019;44:2526–9.
[26] Dutta R, Manzanera S, Gambın-Regadera A, Irles E, Tajahuerce E, Lancis J, Artal P. Single-pixel imaging of the retina through scattering media. Biomed Opt Express 2019;10:4159–67.
[27] Yoneda N, Saita Y, Nomura T. Three-dimensional fluorescence imaging through dynamic scattering media by motionless optical scanning holography. Appl Phys Lett 2021;119:161101.
[28] Tahir H Wang W, Tian L. Adaptive 3D descattering with a dynamic synthesis network. Light Sci Appl 2022;11:42.